

Computational modeling of blood clot lysis considering the effect of vessel wall and pulsatile blood flow

Saleheh Heydari Ghasemi , Mohammad-Taghi Ahmadian *, and Ahmad Assempour 

School of Mechanical Engineering, Sharif University of Technology, Tehran 14588-89694, Iran



(Received 3 May 2023; accepted 1 August 2023; published 5 September 2023)

Stroke is one of the major causes of global death, which can occur due to blockage in a blood vessel by a clot. The immediate dissolving of the clot is essential to restore the blood flow and prevent tissue necrosis. Clot dissolution can be achieved via thrombolytic therapy using plasminogen activators. In this study, a clot dissolution model is developed for a three-dimensional patient-specific carotid artery that investigates the effect of different vessel wall models on clot dissolution. The lysis pattern of the clot and hemodynamics of blood flow are evaluated using three different models of the vessel wall, namely, rigid, linear elastic, and Mooney-Rivlin hyperelastic. The effect of flow condition is considered by solving the Navier-Stokes equations for the free flow domain and the Brinkman equation for the clot domain with the same pressure and velocity fields. This will result in continuous pressure and velocity over the interfaces of the free flow and clot domains. The blood inflow is assumed to be pulsatile. In addition, the species transport driven by diffusion and convection is considered to be different in the porous medium and plasma. The obtained results show that in all models, the starting time of clot volume decrease is almost the same and the clot starts dissolving from the inner curvature of the artery. However, in the hyperelastic model, dissolving the clot takes longer compared to the other two models. By monitoring the vessel wall deformation, the exact time of vessel recanalization is determined.

DOI: [10.1103/PhysRevE.108.034403](https://doi.org/10.1103/PhysRevE.108.034403)

I. INTRODUCTION

Ischemic stroke is one of the leading causes of global death and the most common type of stroke [1]. It is caused by either a thrombus or an embolus. Thrombotic strokes occur when a thrombus develops at a specific site of vessels. To prevent cell necrosis caused by inadequate blood supply to brain cells, the intervention for treatment needs to be very quick. Treatment of patients with thrombus can be performed via medical therapy.

One of the promising treatment procedures in medical therapy is the implementation of the tissue plasminogen activator (tPA) [2]. Intensive studies have been conducted on the biochemistry of thrombolytic therapy and the pharmacodynamics of tPA [3–9]. tPA implementation establishes complex heterogeneous chemical reactions in the vasculature [10]. It activates plasminogen (PLG) and produces plasmin (PLS). PLS degrades the fibrin fibers, and fibrin degradation products (FDPs) are generated. This process neither consumes nor generates tPA. Instead, tPA acts as a catalyst and initiates the reaction. tPA holds great promise in thrombolytic therapy.

Modeling clot lysis is a highly challenging problem due to the complexity of the procedure. It is affected by clot structure, blood flow, kinetic reactions, and the presence of platelets and endothelial cells [11]. Diamond and Anand [10] presented one of the first models of fibrinolysis by solving a set of convection-diffusion-reaction equations, which describes the concentration and transportation of thrombolytic

agents during thrombolytic therapy. They modeled the clot as a porous media formed with a homogeneous concentration of fibrin network. They determined the convective and diffusive transportation as a function of the fiber radius and used Darcy's law to describe one-dimensional fluid flow through the clot. Later, the model was evolved to consider the effect of inhibitors such as $\alpha 2$ -antiplasmin (AP) and plasminogen activator inhibitor-1 (PAI-1) on clot lysis [12,13]. One of the major limitations of their study is disregarding the blood flow and considering lysis as decreasing the fiber radius rather than transverse cutting across fibers.

Wootton *et al.* [14] developed a model to include the influence of the flow condition by taking into account continuity and Navier-Stokes equations. They took into equation the thrombus resistance against fluid flow and quantified the lysis pattern of a mural clot in a semi-occluded vessel. Their results reveal that blood flow accelerates clot lysis.

Recently, to investigate clot dissolution, stochastic models have been established [15,16]. Bannish *et al.* [16] developed a three-dimensional stochastic model which tracks an individual tPA molecule instead of tPA concentration. They indicate that the number of tPA molecules relative to the surface area besides the fiber numbers influences clot lysis.

Pieblags *et al.* [17] presented a computational model which contains a three-dimensional (3D) thrombolysis model and a compartmental model which provide concentration variation of proteins in plasma. The model can assess clot lysis for a specified tPA regimen in a subject-specific geometry. Later, they investigated the influence of clot size and location on clot lysis and recanalization time in a fully occluded vessel [18]. Recently, they expanded their model to evaluate the

*ahmadian@sharif.edu

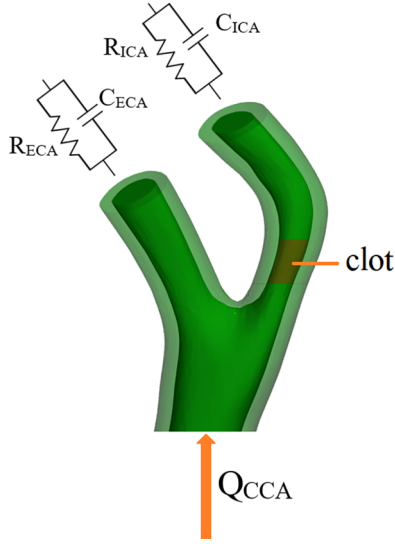


FIG. 1. The reconstructed geometry of the carotid artery.

therapeutic efficacy of various administration regimens of tPA [19].

In cardiovascular fluid mechanics, accurate modeling of fluid-structure interactions (FSI) between blood flow and arterial walls is a major computational challenge. The governing equations must be solved simultaneously and the results are highly dependent on the wall model. A study by Kallekar *et al.* [20] examined the effects of rigid, linear elastic, neo-Hookean, Mooney-Rivlin, and Holzapfel material models of arterial walls on the FSI results under both steady-state and pulsatile flow conditions. However, according to Holzapfel *et al.* [21], arterial walls exhibit high levels of hyperelasticity. Recently, an FSI study was conducted to evaluate hemodynamic parameters at carotid artery bifurcation, which described the vessel wall using linear elastic and hyperelastic material models [22].

This study aims to evaluate clot lysis in the carotid artery bifurcation, considering three different vessel wall models, consisting of rigid, linear elastic, and hyperelastic. The hemodynamics of blood flow and its interaction with solid vessel walls is investigated during tPA administration used in thrombolysis. tPA infusion causes changes in the concentration of species involved in reactions performed in plasma and within the clot. The transport of these species by diffusion and convection in plasma and within the clot is also studied to accurately understand the clot dissolution process.

II. MATERIALS AND METHODS

A. 3D patient-specific arterial geometry

In this study, a 3D patient-specific model of common carotid artery (CCA) bifurcation is constructed from the neck-head computed tomography angiography (CTA) of a 61-year-old male patient, as shown in Fig. 1. The reconstructed geometry consists of CCA, internal carotid artery (ICA), and external carotid artery (ECA). The geometry is exported in Standard Triangle Language (STL) format, and afterwards, an occlusive clot is placed artificially on the base of the ICA using a 3D CAD design software based on clinical

observations. The clot length is 3 mm and its volume is 8.94 mm³. The distance between the front face of the clot and the blood entrance of the CCA is 10 mm. The length of the vessel is 22.3 mm and the thickness of the vessel wall is set to 1 mm. The cross-sectional areas at the CCA inlet, ICA outlet, and ECA outlet are 19.7, 6.1, and 6.62 mm², respectively.

B. Arterial hemodynamics

The blood flow is described by the Navier-Stokes equation in the vessel, and the clot is considered a porous medium made of fibrin fibers. The blood flow through the porous media is described by the Brinkman equation for incompressible fluid [23] as

$$\begin{aligned} \frac{1}{\epsilon_{\text{clot}}}\rho\frac{\partial u_{\text{fluid}}}{\partial t} + \frac{1}{\epsilon_{\text{clot}}}\rho(u_{\text{fluid}} \cdot \nabla)u_{\text{fluid}} - \frac{1}{\epsilon_{\text{clot}}}\nabla \cdot [-pI + K] - (\mu k^{-1})u_{\text{fluid}}, \\ K = \mu \frac{1}{\epsilon_{\text{clot}}}[\nabla u_{\text{fluid}} + (\nabla u_{\text{fluid}})^T], \end{aligned} \quad (1)$$

where u_{fluid} is the fluid velocity, ρ is the fluid density, p is the fluid pressure, ϵ_{clot} is the clot porosity, μ is the blood dynamic viscosity, I is the identity matrix, and k is the clot permeability [24]. Although the Navier-Stokes and Brinkman equations have been used to describe the flow in open and porous regions, respectively, the same fields of velocity and pressure are solved in both domains. Doing so will result in continuous pressure over the interface between the free-flow domain and the porous domain. Also, it enforces the continuity between the fluid velocity in the free-flow domain and the Darcy velocity in the porous one.

The equation of motion for the vessel wall domain is given as

$$\begin{aligned} \rho_s \frac{\partial^2 u_{\text{solid}}}{\partial t^2} &= \nabla \cdot (FS)^T + F_v, \\ F &= I + \nabla u_{\text{solid}}, \\ S &= \frac{\partial W_s}{\partial \epsilon_s}, \end{aligned} \quad (2)$$

where u_{solid} is the solid displacement, ρ_s is the vessel density, F is the deformation gradient tensor, S is the second Piola-Kirchhoff stress, F_v is the volume force, ϵ_s is the Green-Lagrange strain tensor, and W_s is the strain energy function.

To capture the interaction between the blood flow and the solid vessel wall, the force acting on the inner boundary of the vessel and the rate of change in the wall displacement are calculated. The total force exerted on the vessel wall, which is equal to the negative value of the reaction force applied to the fluid, is obtained by

$$f = n \cdot \{-pI + \mu[\nabla u_{\text{fluid}} + (\nabla u_{\text{fluid}})^T]\}, \quad (3)$$

where n is the outward normal to the boundary. The rate of change in the solid displacement, which serves as the moving wall for the blood flow, is calculated as

$$u_{\text{wall}} = \frac{\partial u_{\text{solid}}}{\partial t}. \quad (4)$$

Because the fluid flow and solid equations are formulated in the spatial and material frames, respectively, the arbitrary

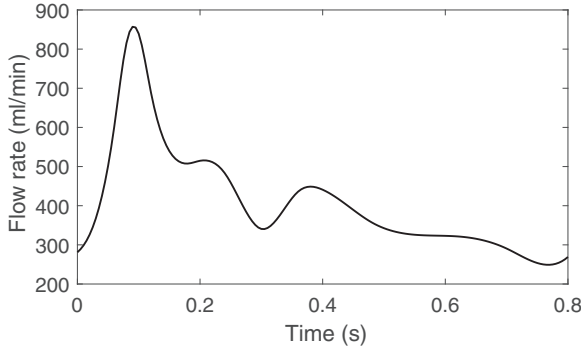


FIG. 2. The blood flow rate applied at the inlet.

Lagrangian-Eulerian (ALE) method is used to describe the fluid-structure interaction at the interface. It should be noted that a force transformation is required because the Navier-Stokes equations and structural mechanics equations are defined in different frames.

In the fluid domain, a pulsatile blood flow rate shown in Fig. 2 is applied at the inlet based on the data from Jonášová *et al.* [25]. The cardiac cycle time is assumed to be 0.8 s. At the outlets, the physiological pressure is applied using the two-element Windkessel model [26]. The two-element Windkessel model describes the relationship between the volumetric outflow and the output pressure as

$$Q(t) = \frac{P(t)}{R} + C \frac{dP(t)}{dt}, \quad (5)$$

and the parameters are calculated based on the method proposed by Jonášová *et al.* [25] and listed in Table I.

The initial values of velocity and pressure are set to zero in the entire geometry and the no-slip boundary condition is used on the vessel walls. For the structural domain, the fixed boundary condition is applied at the entrance and exits of the vessels.

Blood is considered incompressible and Newtonian, and the flow is assumed to be laminar. The dynamic viscosity and density are 0.0037 Pa s and 1050 kg/m³, respectively. The vessel wall is assumed to be homogeneous and isotropic, with a density close to that of the blood; hence it is set to 1050 kg/m³. The mechanical behavior of the vessel wall is simulated using three different models. In the first case, the vessel wall is considered rigid; therefore, its displacements and rotations will be zero in all directions. In the second case, the vessel wall is assumed to be a linear elastic material with Young's modulus of 0.95 MPa and Poisson's ratio of 0.45 [27]. For the last case, the nonlinear five-parameter Mooney-Rivlin material model is used to study the

TABLE I. The two-element Windkessel parameters.

| Parameter | Value |
|-----------|-------------------------------|
| C_{ICA} | 0.199 (mm ³ /Pa) |
| R_{ICA} | 9.897 (Pa s/mm ³) |
| C_{ECA} | 0.215 (mm ³ /Pa) |
| R_{ECA} | 9.230 (Pa s/mm ³) |

TABLE II. The hyperelastic constants used to describe the arterial wall.

| Parameter | Value (kPa) |
|-----------|-------------|
| C_{10} | 50.45 |
| C_{01} | 30.49 |
| C_{20} | 40 |
| C_{02} | 10 |
| C_{11} | 120 |

hyperelastic behavior of the vessel wall. The strain energy function for the hyperelastic model is written as

$$W_s = \sum_{i+j=1}^2 C_{ij}(I_1 - 3)^i(I_2 - 3)^j, \quad (6)$$

where I_1 and I_2 are the first and second invariants of the right Cauchy-Green tensor \mathbf{C} , defined as

$$I_1 = \text{tr } \mathbf{C} \quad I_2 = \frac{1}{2} [I_1^2 - \text{tr } \mathbf{C}^2]. \quad (7)$$

The model parameters are listed in Table II [28].

C. Transport of fibrinolytic proteins in plasma and clot

Blood clot dissolution is a complex process that involves several blood factors. A schematic diagram of the dissolution process is shown in Fig. 3. PLG is a pro-enzyme present in plasma and secreted from the liver. It is activated by tPA and produces PLS, which is the key component in the degradation of fibrin fibers. Two plasma proteins, α 2- antiplasmin (AP) and α 2-macroglobulin (MG), inactivate plasmin in the circulatory system. Also, tPA is inhibited principally by plasminogen activator inhibitor-1 (PAI-1). Another factor that influences thrombolysis is fibrinogen (FBG), the inactivated form of fibrin, which is present at high levels in plasma. The concentration of these species in plasma affects thrombolytic therapy success and recanalization time. Temporal and spatial variation of their concentration is described by the convection-diffusion-reaction equation, written as

$$\frac{\partial c_i}{\partial t} = \nabla \cdot (D_i \nabla c_i) - u_{\text{fluid}} \cdot \nabla c_i + R_i, \quad (8)$$

where c_i is the species concentration in plasma, u_{fluid} is the flow velocity obtained by the Navier-Stokes or Brinkman equations, D_i is the diffusion coefficient which is 5×10^{-11}

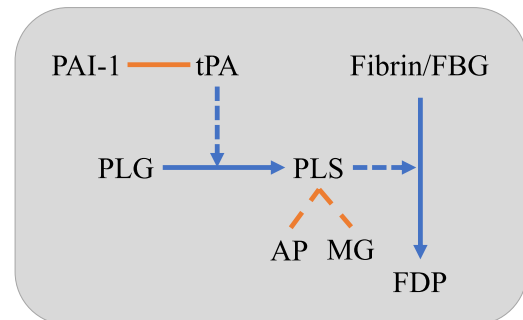


FIG. 3. The schematic illustration of the fibrinolytic reactions.

TABLE III. Reactions between plasma proteins [19].

| No. | Reactions |
|-----|---|
| 1 | $tPA + PLG \xrightarrow{K_{1,M}, k_{1,cat}} tPA + PLS$ |
| 2 | $PLS + AP \xrightleftharpoons[k_{2,r}]{k_{2,f}} PLS \cdot AP \xrightarrow{k_{2,cat}} \text{inactive}$ |
| 3 | $PLS + FBG \xrightarrow{K_{3,M}, k_{3,cat}} PLS + FDP$ |
| 4 | $PLS + MG \xrightarrow{k_4} \text{inactive}$ |
| 5 | $tPA + PAI \xrightarrow{k_5} \text{inactive}$ |

for tPA, PLG, and PLS [29] and 0 for all other factors, and R_i is the reactions performed in plasma. The performed reactions in plasma are listed in Table III. The reaction coefficients and the initial values of species concentration are expressed in the Appendix.

Transport of the species through a porous media is affected by the fluid and matrix properties. Therefore, in the clot domain, the species concentration is described as

$$\frac{\partial(\epsilon_{clot}c_i)}{\partial t} = \nabla \cdot (D_i \nabla c_i) - u_{fluid} \cdot \nabla c_i + \epsilon_{clot} R_i. \quad (9)$$

In the fluid phase of the clot, the reactions are the same as the plasma reactions. In the pore phase of the clot, reactions occur between the bound phase proteins, which will be explained in the next section.

To apply boundary conditions in the transport equations, concentration constraint is used at the inlet. For this purpose, the temporal variation of species concentration in the circulatory system is evaluated according to the method presented by Guet *al.* [19]. Temporal variations of tPA and other fibrinolytic proteins are expressed as follows:

$$\frac{dc_{tPA,sys}}{dt} = -k_{el}c_{tPA,sys} + R_{tPA} + G_{tPA} + \frac{I}{V_c M_{w,tPA}}, \quad (10)$$

$$\frac{dc_{i,sys}}{dt} = -k_{el,i}c_{i,sys} + R_i + G_i, \quad (11)$$

where i refers to PLG, PLS, AP, FBG, MG, and PAI. The first term on the right-hand side of the equations represents the concentration reduction in the plasma due to the half life of the species, and k_{el} is the elimination constant obtained by

$$k_{el,i} = \frac{\ln(2)}{t_{el,i}}, \quad (12)$$

where $t_{el,i}$ is the half life of the i species. The last term on the right-hand side of Eq. (10) represents the increase in tPA concentration because of intravenous infusion of tPA. I is the infusion rate, V_c is the volume of plasma in the circulatory system, and $M_{w,tPA}$ is the molecular weight of tPA. R is the concentration change due to plasma reactions explained in the Appendix, and G is the systemic generation rate of the species given as

$$G_i = k_{el,i}c_{i,0}. \quad (13)$$

Equations (10) and (11) are solved prior to simulation with the fourth-order Runge-Kutta method for the entire simulation time, and then the obtained concentrations are applied as boundary conditions to the transport equations.

TABLE IV. Performed reactions in the pore phase of the clot.

| No. | Reactions |
|-----|--|
| 1 | $tPA + f \xrightleftharpoons[k_{d,tPA}]{k_{a,tPA}} tPA \cdot f$ |
| 2 | $PLG + f \xrightleftharpoons[k_{d,PLG}]{k_{a,PLG}} PLG \cdot f$ |
| 3 | $PLS + f \xrightleftharpoons[k_{d,PLS}]{k_{a,PLS}} PLS \cdot f$ |
| 4 | $tPA \cdot f + PLG \cdot f \xrightarrow{k_M, k_{M,cat}} tPA \cdot f + PLS \cdot f$ |
| 5 | $PLS \cdot f \xrightarrow{k_{deg}} PLS + FDP$ |

^afibrin

D. Lysis model

When tPA and PLG bind to the free binding sites of the clot surface, tPA activates the PLG and produces PLS. PLS degrades fibrin fibers by cutting them transversely. In this process, tPA is not consumed. It is only used as an enzyme to initiate the reaction. PLS can desorb from the clot surface and move into the fluid phase. Additionally, PLS in the fluid phase can resorb to the free binding site of the clot surface. The bound phase reactions performed in the clot are listed in Table IV and reaction coefficients can be found in the Appendix.

The clot lysis model developed by Piebalgs *et al.* [17] is utilized to model clot dissolution. The temporal variation of the bound phase concentration of tPA, PLG, and PLS is described as

$$\frac{\partial n_i}{\partial t} = R_i^{clot}, \quad (14)$$

where i refers to tPA · f, PLG · f, and PLS · f. The concentration change of the total binding sites is written as

$$\frac{\partial n_{tot}}{\partial t} = -k_{deg} \gamma n_{PLS}. \quad (15)$$

The extent of lysis, E_L , is defined to quantify the progress of clot dissolution. It can be determined using the initial and current concentration of binding sites as

$$E_L = 1 - \frac{n_{tot}}{n_{tot,0}}. \quad (16)$$

The initial concentration of binding sites, $n_{tot,0}$, is set to 1.74 μM [19] and the initial bound phase concentration of tPA, PLG, and PLS is set to zero.

Initially, E_L is equal to 0 and, as the dissolution progresses, it increases towards 1. Due to the computational considerations, when the parameter reaches the value of 0.95 [17], named $E_{L_{cr}}$, it is assumed that the clot has fully dissolved in the region and normal blood flow has been restored. If the value of E_L is lower than $E_{L_{cr}}$, the permeability of the clot is determined using Davies' equation [30], which can accurately estimate the permeability of fibrin-rich clots [10]. When the value of E_L exceeds $E_{L_{cr}}$, the permeability will be infinite, which means that the clot element is transformed into the fluid

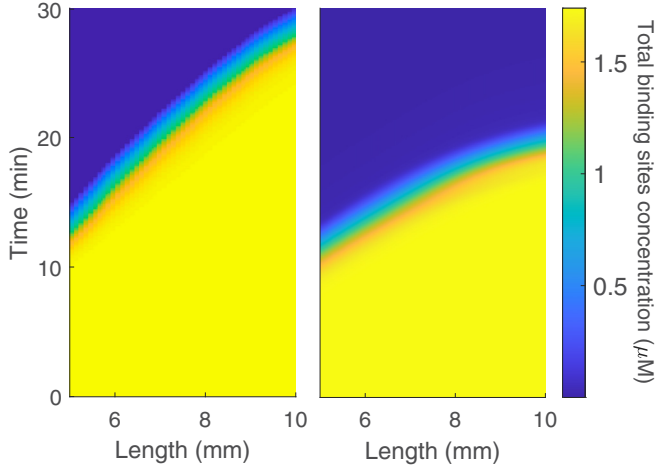


FIG. 4. Comparison of the number of binding sites for the study by Gu *et al.* (left) and present study (right).

element. The permeability of the clot can be written as

$$k = \begin{cases} \frac{4a_f^2}{70(1-\epsilon_{\text{clot}})^{1.5}[1+52(1-\epsilon_{\text{clot}})^{1.5}]}, & E_L < E_{L_{cr}} \\ \infty, & E_L \geq E_{L_{cr}}, \end{cases} \quad (17)$$

where a_f is the fibrin fiber radius in the clot assumed to be 100 nm [31]. The porosity of the clot changes continuously during lysis and it is obtained as

$$\epsilon_{\text{clot}} = 1 - \phi_0(1 - E_L), \quad (18)$$

where ϕ_0 is the initial volume fraction of fibrin. The overall porosity of the clot depends on the clot composition varying from 0.75 for compacted fibrin clots to 0.99 for platelet-retracted clots and fibrin gels [32]. In this study, ϕ_0 is set to 0.05, resulting in a porosity of 0.95.

E. Simulation details

A computational mesh is generated containing 21 510 tetrahedral elements, including 14 103 elements for the vessel wall and 7407 elements for the clot and fluid flow. A set of governing differential equations of fluid flow, solid

vessel walls, species transport, and lysis are solved fully coupled using the finite element method. To solve the equations, the Newton method is applied using the Parallel Space Direct Solver (PARDISO) [33], and the time step selection is performed automatically using the Backward Differentiation Formula (BDF). The total simulation time is 400 seconds, which is sufficient for lysis completion of the clot and flow restoration in all cases. Results are saved every 0.1 second during the simulation. Each simulation required approximately 14 days on an Intel Core i7-10700F desktop PC with 64.0 GB RAM. In addition, the grid independence study is performed by refining the mesh and increasing the number of elements to 61 110.

III. RESULTS

Three simulations are carried out using rigid, linear elastic, and hyperelastic models of vessel walls under the following conditions. Administration of tPA is conducted based on the standard dosing protocol for acute ischemic stroke (AIS) treatment with a high dose of 1.2 mg/kg [18]. Initially, a bolus of 10% tPA is injected within 30 seconds and the remaining 90% is infused continuously for 60 minutes. The high dosage regimen is taken into consideration to accelerate clot lysis and reduce computational costs. To verify the numerical results, the clot lysis process in the study presented by Gu *et al.* [19] is resimulated using our model. In this two-dimensional simulation, the dissolution of a 5 cm clot in a vessel with a length of 10 cm is modeled for 30 min. Figure 4 shows the number of binding sites along the clot length at different times compared with the results of Gu *et al.* As can be observed in the figure, the results are in good agreement. The results indicate a similar pattern, but the number of binding sites decreases more rapidly in our model, which will be discussed later in Sec. IV.

A. Clot volume and porosity

The progress of clot dissolution is evaluated by the clot volume. Figure 5(a) shows the changes in clot volume with respect to time throughout the simulations. As can be observed in the figure, the clot volume remains constant for the first few minutes and then starts to decrease at approximately

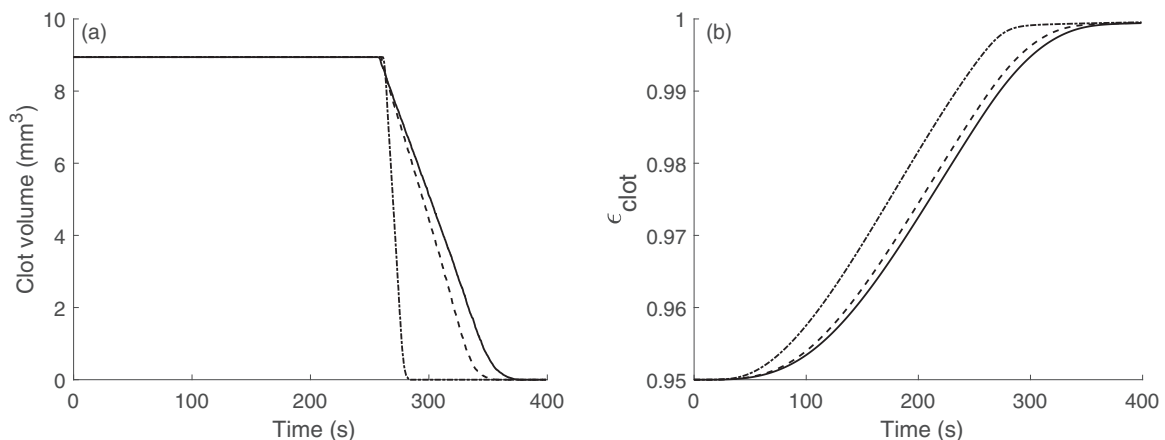


FIG. 5. Changes in (a) clot volume and (b) clot porosity during tPA administration, in rigid (dotted line), linear elastic (dashed line), and hyperelastic (solid line) vessel wall models.

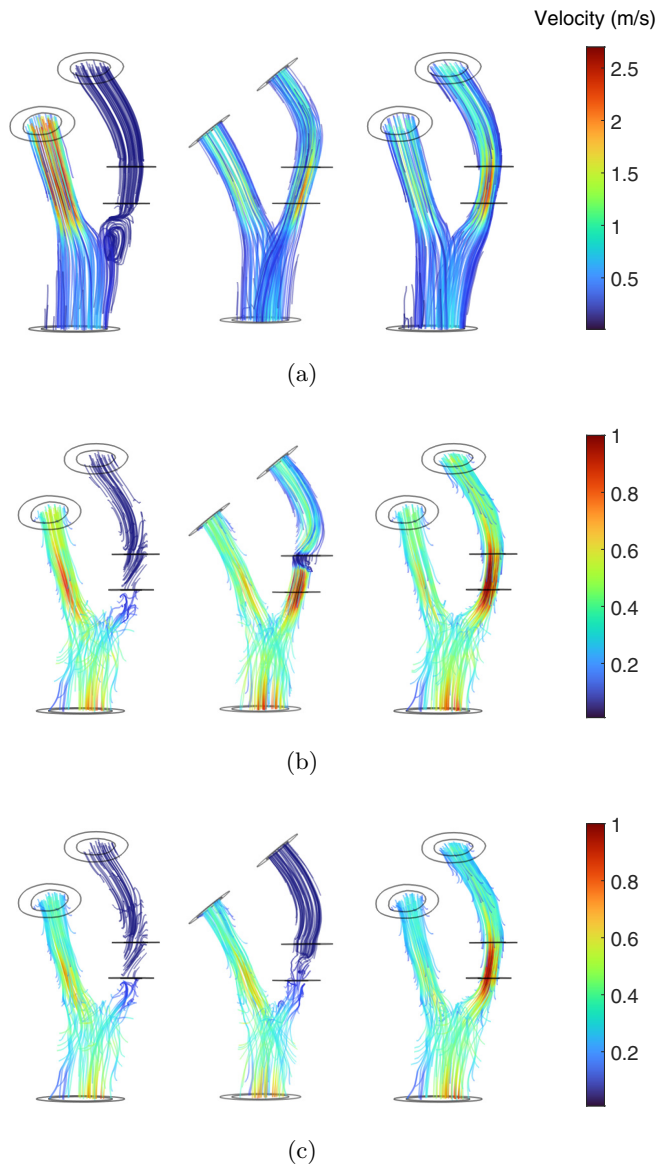


FIG. 6. Velocity streamlines in different vessel wall models: (a) rigid, (b) linear elastic, and (c) hyperelastic, at 10 s (left), 320 s (middle), and 400 s (right).

260 seconds after tPA administration in all cases. Afterwards, the clot volume decreases linearly until the dissolution approaches completion and, at this point, the lysis starts to slow down. This decrease in the dissolution rate can be due to the recanalization of the vessel, which reduces the pressure gradient required for the flow. The clot is fully dissolved after 284, 358, and 378 seconds in the rigid, linear, and hyperelastic vessel wall models, respectively.

Although the volume of the clot does not change in the first few minutes after tPA administration, the porosity of the clot starts to increase from the early stages, as shown in Fig. 5(b). The initial porosity is assumed to be 0.95 at the beginning of the simulation [32], and Fig. 5(b) shows the change in its average over time. The average porosity gradually increases after tPA infusion in all cases. As the porosity increases, the clot permeability improves. Consequently, the blood flow speed

within the clot accelerates, boosting the convection within the clot. This, in turn, increases the rate of change in porosity. As the lysis approaches completion, the rate of increase in porosity drops due to recanalization.

B. Hemodynamics of blood flow

Figure 6 shows the velocity profile in the fluid flow domain at 10, 320, and 400 seconds. At the early stages of the simulation, because the clot is located at the base of the ICA, no flow passes through this branch and it all rushes through the ECA branch, which is shown in the figure at $t = 10$ seconds. As the porosity of the clot increases gradually due to the tPA administration, over time, the clot volume starts to decrease until the breakthrough occurs in the inner curvature of the ICA branch, and the flow is partially restored. At this point, the flow passes through the ICA with a high-velocity jet. As the lysis progresses, the clot is fully dissolved and the normal flow is recovered in the vessel. As shown in the figure, at $t = 320$ seconds, the clot is fully dissolved in the rigid wall model, but in the other two models, it is partially dissolved. At $t = 400$ seconds, the blood clot is dissolved completely in all the models and the normal flow is restored.

As expected, in the rigid model, contrary to the other two models, the velocity of the fluid in contact with the vessel wall is zero. In addition, the maximum fluid velocity in the rigid model is much higher than that of the other two models. The blood velocity in the linear elastic and hyperelastic models is more consistent with experimental measurements, which reported it to be less than 125 cm/s in ICA [34].

C. Concentration of lysis components within the clot

The concentrations of the free phase tPA and PLG are illustrated in Fig. 7. As shown in Fig. 7(a), after the bolus injection, the concentration of tPA rapidly increases within the clot and, owing to the continuous infusion over 60 minutes, it continues to rise to the maximum value and remains constant afterwards. Since the fluid velocity in the hyperelastic model is lower than the other models, it takes longer for the tPA concentration within the clot to reach its maximum value, and thus the dissolution process will be more time consuming. Figure 7(b) shows the PLG concentration within the clot. As shown in the figure, the PLG concentration in plasma decreases at the beginning of the simulation and its rate of decrease in the rigid model is lower compared to the other two models. This concentration reduction is due to the reaction with tPA, as well as its absorption to the surface of the clot. After approximately 80 seconds, the PLG concentration in the linear elastic and hyperelastic models is lower than in the rigid model due to its greater absorption on the surface of the clot. In these two models, after about 150 seconds, the PLG concentration starts to increase. This is because of an increase in desorption from the clot surface when the level of bound phase concentration is high.

The temporal and spatial variation of the bound phase tPA in mol/m^3 is illustrated in Fig. 8. As can be observed in the figure, in all the time points, the spatial variation of n_{tPA} in the rigid vessel wall model is uniform in contrast to

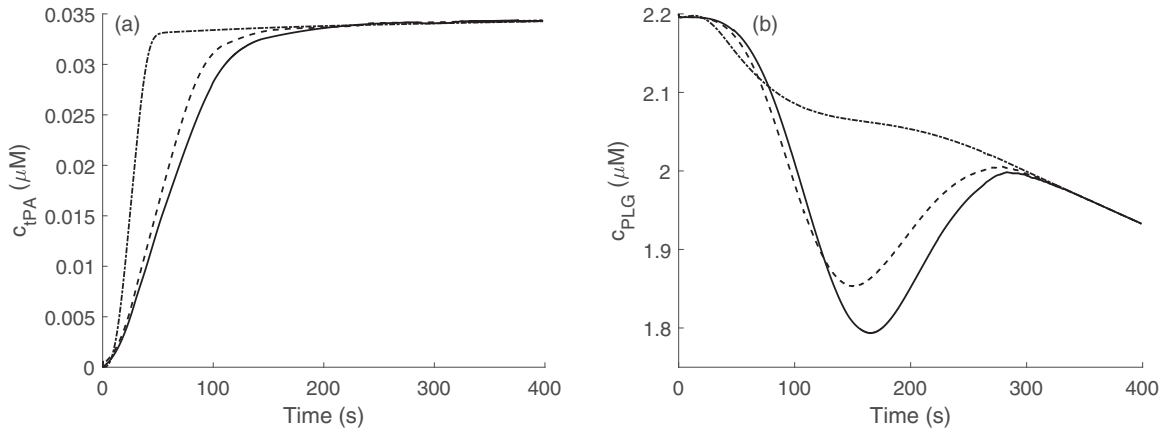


FIG. 7. Changes in the concentration of (a) tPA and (b) PLG within the clot during tPA administration in rigid (dotted line), linear elastic (dashed line), and hyperelastic (solid line).

the other two vessel wall models. At 10 seconds, the spatial variation of n_{tPA} is uniform and low in all cases. After 150 seconds in the linear elastic and hyperelastic vessel wall models, the concentration of n_{tPA} is high at the clot front and it decreases toward the distal end of the clot. At 250 seconds, the concentration of bound phase tPA has increased compared to the previous times and its distribution has a similar pattern as the 150 seconds. At 300 seconds, the clot is fully dissolved in the rigid vessel wall model. However, in the linear elastic and hyperelastic vessel wall models, the clot is partially dissolved and the concentration of n_{tPA} decreases throughout the clot. This concentration reduction can be explained by the fact that when the bound phase concentration is high, the rate of desorption of the tPA molecules from the clot is higher than the rate of their adhesion to the clot. At 350 seconds, the clot is fully dissolved in the linear elastic vessel wall model, and in the hyperelastic model, the vessel is recanalized, but the clot has not disappeared completely.

D. Arterial deformation

The arterial deformation in the CCA and ECA in the linear elastic and hyperelastic vessel wall models is shown in Fig. 9. As can be observed from the figure, when the vessel wall is assumed to be hyperelastic, its deformation is higher than when it is linear elastic. The periodic behavior of arterial deformation is due to the pulsatile blood flow rate applied at the inlet, and there is a proportional relationship between their values. It is evident that after 320 and 335 seconds of the simulation in linear elastic and hyperelastic vessel wall models, respectively, the arterial deformation decreases by about 15%; however, the pattern remains unchanged. It is the exact time point when the recanalization occurs, which causes lower stress on the vessel wall and lower deformation.

E. Wall shear stress

Wall shear stress (WSS) at 10 and 400 s is demonstrated in Fig. 10. As mentioned before, as long as the clot blocks the ICA branch, the blood flow does not pass through it and

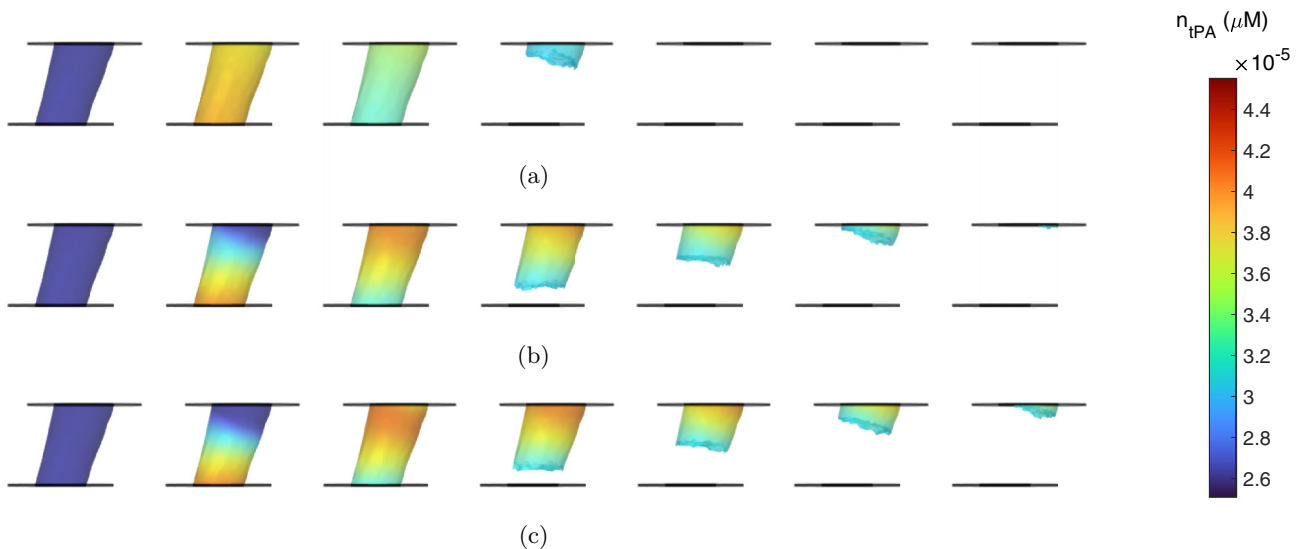


FIG. 8. Concentration of bound phase tPA in (a) rigid, (b) linear elastic, (c) hyperelastic vessel wall models at $t = 10, 150, 250, 275, 300, 325,$ and 350 seconds, from left to right.

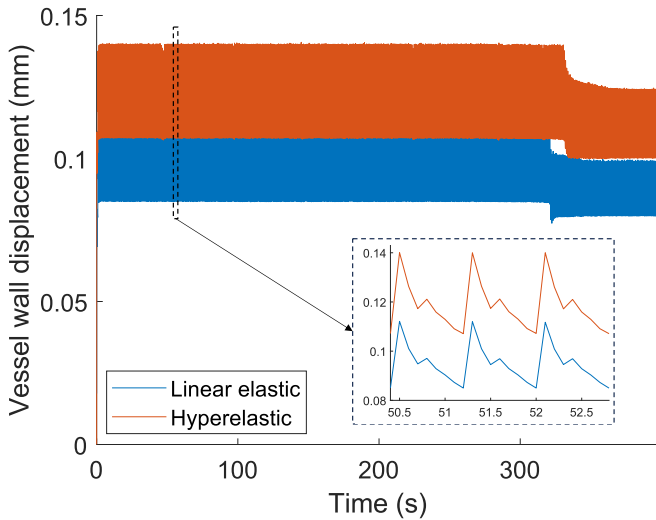


FIG. 9. Vessel wall displacement in linear elastic (blue) and hyperelastic (orange) wall models.

therefore no WSS is applied at the ICA branch wall. It can be observed from the figure that at $t = 10$ s, in the rigid model, the highest amount of WSS occurs at the ECA branch and in the other two models at the bifurcation. At the end of the simulation, in all three models, the maximum value of WSS occurs at the ICA due to the decrease in the cross-sectional area of the vessel caused by the clot. It is worth noting that in the rigid model, the maximum WSS is noticeably higher than that in the other two models.

IV. DISCUSSION

This study investigated the effect of vessel wall models and pulsatile blood flow on the dissolution of an occlusive clot. As shown in Fig. 5(a), the decrease in clot volume shows a linear time dependence, which is in agreement with the experiments conducted by Bizjak *et al.* [35]. The figure also shows that the complete lysis time of the clot in the hyperelastic model is longer than that of the linear elastic and rigid models by approximately 1.06 and 1.3, respectively. Since Tratar *et al.* demonstrated that high speeds of blood flow accelerate clot lysis [36], the longer lysis time in the hyperelastic model can be due to the lower flow velocity in the presence of occlusion, as shown in Fig. 6. Lower flow velocity causes the concentration of tPA within the clot to reach its maximum value in a longer time frame. By comparing the results of our rigid wall model with previous studies by Piebalgs *et al.* [17] and Gu *et al.* [18], it is found that the clot dissolution is faster in our model due to considering the blood flow pulsatile.

The lysis completion time of the clot in this research is reported to be 284, 358, and 378 seconds in rigid, linear elastic, and hyperelastic vessel wall models, respectively. Christou *et al.* [37] found that 25% of the patients who received tPA treatment achieved partial or complete recanalization in 30 minutes. Also, by monitoring the clot dissolution process in patients treated with tPA using transcranial Doppler (TCD), Alexandrov [2] classified the recanalization time as sudden, stepwise, and slow. Recanalization was sudden (<1 minute)

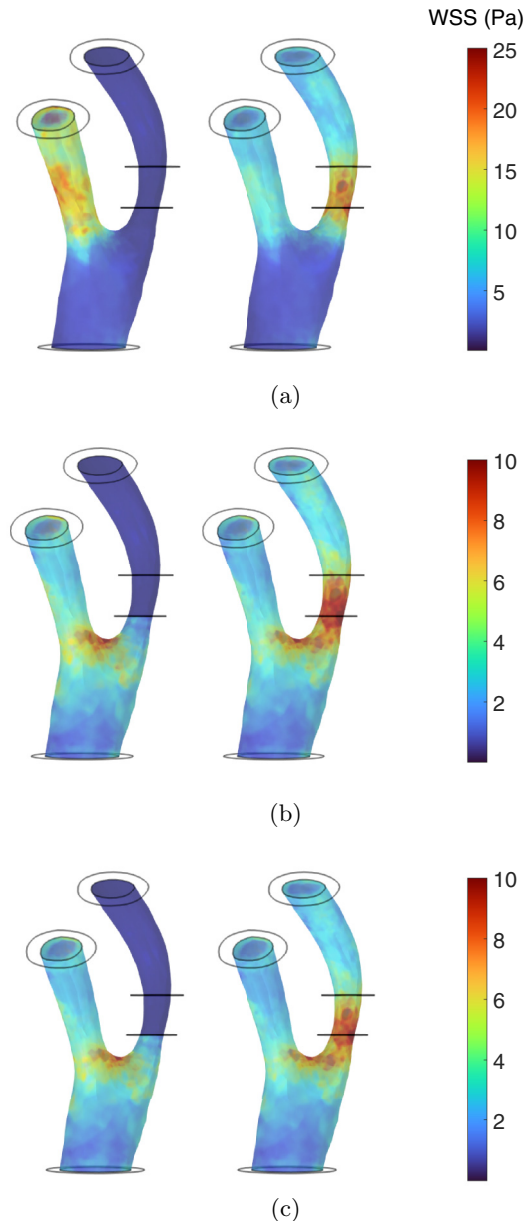


FIG. 10. WSS in (a) rigid, (b) linear elastic, and (c) hyperelastic vessel wall models at 10 s (left) and 400 s (right).

in 12% of patients, stepwise (over 1 to 29 minutes) in 53% of patients, and slow (>30 minutes) in 35% of patients. They reported a mean recanalization time of 23 ± 16 minutes. Another study conducted by Elder *et al.* reported that ICA reperfusion time in patients who receive tPA is approximately 25 min [38]. As experimental results reveal, the clot dissolution time can vary from sudden to slow; however, it is clear that the clot lysis time in our simulation is lower than the average time presented in the experiments. There are two possible explanations for this difference. First, the clot structure in our simulation only consists of a fibrin network, whereas in practice it contains platelets and erythrocytes that decrease the clot permeation and slow down the lysis. Second, because of computational limitations, the clot is relatively smaller in volume compared to experimental studies. According to

Yoo *et al.*, patients who did not undergo successful recanalization had an average clot volume of 149.5 mm³ [39], which is significantly higher than the considered volume in this study. In addition, we adopted the high dosage regimen of tPA, while the required dose for each patient should be determined based on FBG concentration in plasma to reduce the risk of bleeding.

Previous studies [17,18], which modeled clot lysis without considering the effect of the vessel wall, showed that the clot dissolution is asymmetric and breakthrough occurs along the inner curvature of the vessel. In our simulations, regardless of the wall model, the dissolution of the clot was also asymmetric and vessel recanalization occurred along the inner curvature of the ICA branch. The geometric model of the vessel is such that it directs the flow towards the inner curvature of the ICA branch, as shown in Fig. 6 at 320 seconds. Dissolving from the inner curvature of the vessel happens due to the flow recirculation, which prolongs the stay of tPA in that area [18]. The concentration of bound phase tPA within the clot shown in Fig. 8 at 150 and 250 seconds is also higher in the inner than the outer curvature. The asymmetric lysis can cause a mural clot, which not only leads to clot reformation in this area, but also the possibility of embolism increases when these fragments are detached from the vessel wall.

tPA concentration in plasma increases by intravenous infusion, resulting in an increase in the bound phase concentration of tPA within the clot. The spatial distribution of the bound phase concentration of tPA in the rigid wall model is uniform, which is in good agreement with the study by Piebalgs *et al.* [17]. However, in the other two models, the binding of tPA molecules to the clot is nonuniform. After tPA administration, tPA concentration in plasma increases; the molecules gather on the surface of the clot and bind to the fibrin fibers on the surface of the clot, causing them to degrade. Several experiments mimic the clot dissolution process by adding tPA. These studies showed that the lytic enzymes have a high accumulation at the clot front, and the lysis proceeds through the front side of the clot [40–42]. Fibrin fiber degradation increases the porosity on the surface of the clot, which accelerates the penetration of tPA molecules and other fibrinolytic proteins into the clot. With more tPA penetration, the bound phase concentration of tPA within the clot also increases and further boosts the clot dissolution. After the porosity increases on the surface of the clot and the number of fibrin strands decreases, the bound phase concentration also decreases. As shown in Fig. 8, at 250 seconds, on the surface of the clot, the bound phase concentration is lower than in other regions. This process continues until the clot is completely dissolved.

In a study conducted by Kumar *et al.* [22], it has been shown that WSS rises with increasing stiffness in linear elastic models. In our simulation, the WSS values in the rigid wall model are higher than in the other two models, and the hyperelastic wall model has the lowest WSS values. After vessel recanalization in all models, WSS has its maximum value in the region where the clot was located due to the reduction of the ICA cross-sectional area. Also, in the linear elastic and hyperelastic models, the value of WSS is high at the bifurcation, which is due to the geometry of the vessel and flow division.

V. CONCLUSIONS

In this paper, we investigated the dissolution of a blood clot considering the effect of the vessel wall by a two-way coupled FSI simulation. The vessel wall was modeled with three types of materials: rigid, linear elastic, and Mooney-Rivlin hyperelastic. The results showed that in the hyperelastic model, which is a more realistic model, the complete dissolution of the clot took 1.3 times longer than that in the rigid case. Also, the lysis time for hyperelastic and linear elastic models was almost the same. As long as recanalization did not occur in ICA, the blood flow velocity in the ECA in the rigid model was much higher than the other two models and exceeded the biological range, while in the linear elastic and hyperelastic models, even with occlusion, the velocity remained within the biological range. In the future, a more accurate model of the clot structure, which consists of blood cells and platelets, can be presented, and more physiological factors that affect the clot dissolution process can be considered. Also, the blood flow was assumed to be laminar; however, it may be turbulent in some moments after the vessel recanalization, which can be investigated for its effect on the lysis process.

APPENDIX:

The R term for different species in Eqs. (10) and (11) is obtained as follows [19]:

$$R_{tPA} = -k_5 c_{tPA} c_{PAI}, \quad (A1)$$

$$R_{PLG} = -\frac{k_{1,cat} c_{tPA} c_{PLG}}{K_{1,M} + c_{PLG}}, \quad (A2)$$

$$R_{PLS} = \frac{k_{1,cat} c_{tPA} c_{PLG}}{K_{1,M} + c_{PLG}} - k_{2,f} c_{PLS} c_{AP} \quad (A3)$$

$$+ k_{2,r} c_{PLS.AP} - k_4 c_{PLS} c_{MG}, \quad (A4)$$

$$R_{FBG} = -\frac{k_{3,cat} c_{PLS} c_{FBG}}{K_{3,M} + c_{FBG}},$$

$$R_{PLS.AP} = k_{2,f} c_{PLS} c_{AP} - k_{2,cat} c_{PLS.AP} - k_{2,r} c_{PLS.AP}, \quad (A5)$$

$$R_{AP} = -k_{2,f} c_{PLS} c_{AP} + k_{2,r} c_{PLS.AP}, \quad (A6)$$

$$R_{MG} = -k_4 c_{PLS} c_{MG}, \quad (A7)$$

$$R_{PAI} = -k_5 c_{tPA} c_{PAI}. \quad (A8)$$

The reaction coefficients and the initial values of species concentration of the free phase are listed in Table V and Table VI, respectively [17,19].

The reaction coefficients of the bound phase concentrations are listed in Table VII [17,19].

TABLE V. Reaction coefficients performed in plasma.

| Parameter | Value | Parameter | Value |
|-------------|----------------------------|-------------|------------------------------|
| $k_{1,m}$ | 28 (μM) | $k_{3,m}$ | 30 (μM) |
| $k_{1,cat}$ | 0.3 (1/s) | $k_{3,cat}$ | 250 (1/s) |
| $k_{2,f}$ | 10 [1/($\mu\text{M s}$)] | k_4 | 0.35 [1/($\mu\text{M s}$)] |
| $k_{2,r}$ | 0.0021 (1/s) | k_5 | 37 [1/($\mu\text{M s}$)] |
| k_2 | 0.004 (1/s) | | |

TABLE VI. Initial values of species concentration in plasma.

| Parameter | Value (μM) | Parameter | Value (μM) |
|--------------------|-------------------------|--------------------|-------------------------|
| $C_{\text{tPA},0}$ | 0.05×10^{-3} | $C_{\text{AP},0}$ | 1 |
| $C_{\text{PLG},0}$ | 2.2 | $C_{\text{MG},0}$ | 3 |
| $C_{\text{PLS},0}$ | 0 | $C_{\text{PAI},0}$ | 0.523×10^{-3} |
| $C_{\text{FBG},0}$ | 8 | | |

TABLE VII. Reaction coefficients performed in the pore phase of the clot.

| Parameter | Value | Parameter | Value |
|--------------------|------------------------------|--------------------|------------------------|
| $k_{a,\text{tPA}}$ | 0.01 [1/($\mu\text{M s}$)] | $k_{d,\text{PLS}}$ | 0.05 (1/s) |
| $k_{d,\text{tPA}}$ | 0.0058 (1/s) | k_m | 0.16 (μM) |
| $k_{a,\text{PLG}}$ | 0.1 [1/($\mu\text{M s}$)] | $k_{m,\text{cat}}$ | 0.3 (1/s) |
| $k_{d,\text{PLG}}$ | 3.8 (1/s) | k_{deg} | 2.178 (1/s) |
| $k_{a,\text{PLS}}$ | 0.1 [1/($\mu\text{M s}$)] | | |

- [1] A. Durukan and T. Tatlisumak, Acute ischemic stroke: Overview of major experimental rodent models, pathophysiology, and therapy of focal cerebral ischemia, *Pharmacol. Biochem. Behav.* **87**, 179 (2007).
- [2] A. V. Alexandrov, W. S. Burgin, A. M. Demchuk, A. El-Mitwalli, and J. C. Grotta, Speed of intracranial clot lysis with intravenous tissue plasminogen activator therapy: Sonographic classification and short-term improvement, *Circulation* **103**, 2897 (2001).
- [3] N. Bizjak, F. Bajd, J. Vidmar, A. Blinc, M. P. Perme, V. J. Marder, V. Novokhatny, and I. Serša, Direct microscopic monitoring of initial and dynamic clot lysis using plasmin or rt-PA in an *in vitro* flow system, *Thromb. Res.* **133**, 908 (2014).
- [4] K. R. Godfrey, P. Tanswell, R. A. Bates, M. J. Chappell, and F. N. Madden, Nonlinear pharmacokinetics of tissue-type plasminogen activator in three animal species: A comparison of mathematical models, *Biopharm. Drug Dispos.* **19**, 131 (1998).
- [5] C. Pleydell, T. David, S. Smye, and D. Berridge, A mathematical model of post-canalization thrombolysis, *Phys. Med. Biol.* **47**, 209 (2002).
- [6] I. Serša, G. Tratar, and A. Blinc, Blood clot dissolution dynamics simulation during thrombolytic therapy, *J. Chem. Inf. Model.* **45**, 1686 (2005).
- [7] I. Serša, G. Tratar, U. Mikac, and A. Blinc, A mathematical model for the dissolution of nonocclusive blood clots in fast tangential blood flow, *Biorheology* **44**, 1 (2007).
- [8] P. Tanswell, G. Heinzel, A. Greischel, and J. Krause, Nonlinear pharmacokinetics of tissue-type plasminogen activator in three animal species and isolated perfused rat liver, *J. Pharmacol. Expt. Therapeut.* **255**, 318 (1990).
- [9] A. Tiefenbrunn, R. Graor, A. Robison, F. Lucas, A. Hotchkiss, and B. Sobel, Pharmacodynamics of tissue-type plasminogen activator characterized by computer-assisted simulation, *Circulation* **73**, 1291 (1986).
- [10] S. L. Diamond and S. Anand, Inner clot diffusion and permeation during fibrinolysis, *Biophys. J.* **65**, 2622 (1993).
- [11] K. Kolev and R. Machovich, Molecular and cellular modulation of fibrinolysis, *Thromb. Haemostas.* **89**, 610 (2003).
- [12] S. Anand, V. Kudallur, E. Bruce Pitman, and S. L. Diamond, Mechanisms by which thrombolytic therapy results in nonuniform lysis and residual thrombus after reperfusion, *Ann. Biomed. Eng.* **25**, 964 (1997).
- [13] S. Anand, J.-H. Wu, and S. L. Diamond, Enzyme-mediated proteolysis of fibrous biopolymers: Dissolution front movement in fibrin or collagen under conditions of diffusive or convective transport, *Biotechnol. Bioeng.* **48**, 89 (1995).
- [14] D. M. Wootton, A. S. Popel, and B. Rita Alevriadou, An experimental and theoretical study on the dissolution of mural fibrin clots by tissue-type plasminogen activator, *Biotechnol. Bioeng.* **77**, 405 (2002).
- [15] B. E. Bannish, I. N. Chernysh, J. P. Keener, A. L. Fogelson, and J. W. Weisel, Molecular and physical mechanisms of fibrinolysis and thrombolysis from mathematical modeling and experiments, *Sci. Rep.* **7**, 6914 (2017).
- [16] B. E. Bannish, J. P. Keener, and A. L. Fogelson, Modelling fibrinolysis: A 3d stochastic multiscale model, *Math. Med. Biol.: J. IMA* **31**, 17 (2014).
- [17] A. Piebalgs, B. Gu, D. Roi, K. Lobotesis, S. Thom, and X. Y. Xu, Computational simulations of thrombolytic therapy in acute ischaemic stroke, *Sci. Rep.* **8**, 15810 (2018).
- [18] B. Gu, A. Piebalgs, Y. Huang, D. Roi, K. Lobotesis, C. Longstaff, A. D. Hughes, R. Chen, S. A. Thom, and X. Y. Xu, Computational simulations of thrombolysis in acute stroke: Effect of clot size and location on recanalisation, *Med. Eng. Phys.* **73**, 9 (2019).
- [19] B. Gu, A. Piebalgs, Y. Huang, C. Longstaff, A. D. Hughes, R. Chen, S. A. Thom, and X. Y. Xu, Mathematical modelling of intravenous thrombolysis in acute ischaemic stroke: Effects of dose regimens on levels of fibrinolytic proteins and clot lysis time, *Pharmaceutics* **11**, 111 (2019).
- [20] L. Kallekar, C. Viswanath, and M. Anand, Effect of wall flexibility on the deformation during flow in a stenosed coronary artery, *Fluids* **2**, 16 (2017).
- [21] G. A. Holzapfel, G. Sommer, C. T. Gasser, and P. Regitnig, Determination of layer-specific mechanical properties of human coronary arteries with nonatherosclerotic intimal thickening and related constitutive modeling, *Am. J. Physiol.-Heart Circulat. Physiol.* **289**, H2048 (2005).
- [22] N. Kumar, R. Pai, M. Manjunath, A. Ganesha, and S. Abdul Khader, Effect of linear and Mooney-Rivlin material model on carotid artery hemodynamics, *J. Braz. Soc. Mech. Sci. Eng.* **43**, 395 (2021).
- [23] D. A. Nield and A. Bejan, *Convection in Porous Media* (Springer, Cham, 2017).
- [24] A. R. Wufsus, N. Macera, and K. Neeves, The hydraulic permeability of blood clots as a function of fibrin and platelet density, *Biophys. J.* **104**, 1812 (2013).
- [25] A. Jonášová and J. Vimmr, Noninvasive assessment of carotid artery stenoses by the principle of multiscale modelling of non-newtonian blood flow in patient-specific models, *Appl. Math. Comput.* **319**, 598 (2018).

- [26] N. Westerhof, J.-W. Lankhaar, and B. E. Westerhof, The arterial windkessel, *Med. Biol. Eng. Comput* **47**, 131 (2009).
- [27] A. V. Kamenskiy, Y. A. Dzenis, J. N. MacTaggart, T. G. Lynch, S. A. J. Kazmi, and I. I. Pipinos, Nonlinear mechanical behavior of the human common, external, and internal carotid arteries in vivo, *J. Surg. Res.* **176**, 329 (2012).
- [28] A. Creane, E. Maher, S. Sultan, N. Hynes, D. J. Kelly, and C. Lally, Finite element modelling of diseased carotid bifurcations generated from *in vivo* computerised tomographic angiography, *Comput. Biol. Med.* **40**, 419 (2010).
- [29] K. M. Weigandt, N. White, D. Chung, E. Ellingson, Y. Wang, X. Fu, and D. C. Pozzo, Fibrin clot structure and mechanics associated with specific oxidation of methionine residues in fibrinogen, *Biophys. J.* **103**, 2399 (2012).
- [30] C. Davies, The separation of airborne dust and particles, *Proc. Inst. Mech. Eng.* **167**, 185 (1953).
- [31] C. Yeromonahos, B. Polack, and F. Caton, Nanostructure of the fibrin clot, *Biophys. J.* **99**, 2018 (2010).
- [32] S. L. Diamond, Engineering design of optimal strategies for blood clot dissolution, *Annu. Rev. Biomed. Eng.* **1**, 427 (1999).
- [33] O. Schenk and K. Gärtner, Solving unsymmetric sparse systems of linear equations with pardiso, *Future Generat. Comput. Syst.* **20**, 475 (2004).
- [34] M. Özdikici, Quantitative measurements of blood flow parameters in normal internal carotid arteries with color doppler ultrasonography and vascular stenosis index of stenotic vessels, *Clinic. Med. Med. Res.* **1**, 01 (2020).
- [35] N. Bizjak, F. Bajd, J. Vidmar, A. Blinc, V. J. Marder, V. Novokhatny, and I. Serša, Comparison of local thrombolytic efficacy of plasmin and rt-PA in an *in vitro* flow system; A pilot study, *Blood Coagulat. Fibrinolys.* **24**, 711 (2013).
- [36] G. Tratar, A. Blinc, M. Štrukelj, U. Mikac, and I. Serša, Turbulent axially directed flow of plasma containing rt-PA promotes thrombolysis of non-occlusive whole blood clots *in vitro*, *Thromb. Haemostas.* **91**, 487 (2004).
- [37] I. Christou, A. V. Alexandrov, W. S. Burgin, A. W. Wojner, R. A. Felberg, M. Malkoff, and J. C. Grotta, Timing of recanalization after tissue plasminogen activator therapy determined by transcranial doppler correlates with clinical recovery from ischemic stroke, *Stroke* **31**, 1812 (2000).
- [38] T. A. Elder, L. H. Verhey, H. Schultz, E. S. Smith, and J. G. Adel, Cervical carotid occlusion in acute ischemic stroke: Should we give tpa? *Surgic. Neurol. Intl.* **13**, 177 (2022).
- [39] J. Yoo, J.-H. Baek, H. Park, D. Song, K. Kim, I. G. Hwang, Y. D. Kim, S. H. Kim, H. S. Lee, S. H. Ahn *et al.*, Thrombus volume as a predictor of nonrecanalization after intravenous thrombolysis in acute stroke, *Stroke* **49**, 2108 (2018).
- [40] J. Collet, D. Park, C. Lesty, J. Soria, C. Soria, G. Montalescot, and J. Weisel, Influence of fibrin network conformation and fibrin fiber diameter on fibrinolysis speed: Dynamic and structural approaches by confocal microscopy, *Arterioscleros. Thromb. Vascul. Biol.* **20**, 1354 (2000).
- [41] D. V. Sakharov and D. C. Rijken, Superficial accumulation of plasminogen during plasma clot lysis, *Circulation* **92**, 1883 (1995).
- [42] D. V. Sakharov, J. F. Nagelkerke, and D. C. Rijken, Rearrangements of the fibrin network and spatial distribution of fibrinolytic components during plasma clot lysis: Study with confocal microscopy, *J. Biol. Chem.* **271**, 2133 (1996).